High-efficiency photon capturing in ultrathin silicon solar cells with front nanobowl texture and truncated-nanopyramid reflector

Zhenhai Yang,[1,2] Xiaofeng Li,[1,2,4] Shaolong Wu,[1,2] Pingqi Gao,[3] and Jichun Ye[3,5]

[1]*College of Physics, Optoelectronics and Energy & Collaborative Innovation Center of Suzhou Nano Science and Technology, Soochow University, Suzhou 215006, China*

[2]*Key Lab of Advanced Optical Manufacturing Technologies of Jiangsu Province & Key Lab of Modern Optical Technologies of Education Ministry of China, Soochow University, Suzhou 215006, China*

[3]*Ningbo Institute of Material Technology and Engineering, Chinese Academy of Sciences, Ningbo 315201, China*

[4]*e-mail: xfli@suda.edu.cn*

[5]*e-mail: jichun.ye@nimte.ac.cn*

Received November 14, 2014; revised January 22, 2015; accepted January 22, 2015; posted January 28, 2015 (Doc. ID 226894); published March 12, 2015

We present a crystalline siliconthin-film (5 μm) solar cell decorated by a front nanobowled texture and a rear truncated-nanopyramid silver reflector. This design substantially suppresses the overall light reflection and enhances the optical resonances inside the silicon film leading to the photon-capturing performance comparable to the Yablonovitch limit. We show that optical absorption can be greatly improved by adjusting the ratio of the periods between the rear and front nanostructures with an optimal ultimate photocurrent density around 35.3 mA/cm^2 and an enhancement of 42.6% relative to the planar counterpart. A thorough optoelectronic simulation predicts the light-conversion efficiency of around 15.5%, i.e., 67.3% higher than that of the planar system.

An efficient photon-capturing scheme, which plays a significant role in reducing the production cost (i.e., small volume consumption and low requirement of the purity of the photoactive material), is one of the foremost challenges in realizing crystalline silicon (c-Si) thin-film solar cells (TFSCs). This is because Si has a low absorption coefficient limited by the intrinsic indirect band structure and thus requires a thickness of around 150–300 μm for high-performance solar cells. Owing to the excellent photon-capturing ability of nanophotonic structures, researchers demonstrated that fabricating high-efficiency c-Si solar cells with a thickness of 20 μm or thinner becomes a prospective reality [1,2].

In order to supress the cell reflection, front nanostructures (e.g., nanoparticles, plasmonics, photonic crystals) are often introduced to serve as the antireflecting or forward-scattering components [3–8]. For example, Zhang *et al.* proposed a novel nanocone design that greatly enhances the light absorption of c-Si TFSCs, especially in the wavelength range of 300–550 nm, leading to an ultimate efficiency of ~28% under a period of 559 nm and a height of 500 nm [9]. Recently, rear nanostructures have also been demonstrated to be vital in improving the long-wavelength light-trapping performance of TFSCs [1,2,10–12]. However, to realize a broadband absorption enhancement, doublely configured nanostructures seem to be more effective [13–16]. For instance, Ken *et al.* showed that double nanocone structures can improve the absorption substantially. They yield an optimized photocurrent up to 34.6 mA/cm^2 at an equivalent thickness of 2 μm under an ideal condition of a perfect electric conductor [17]. Based on this idea Shi *et al.* found that the huge enhancement in light absorption can also be achieved by using the nanostructure with top nanopyramids and rear-located silver (Ag) nanoparticles [18]. For absorption performance only, the designing guiderline for double-side textures is to minimize the reflection at the front and simultaneously maximum the diffraction-related light trapping at the rear. However, considering the final power-conversion efficiency, there is always an imbalance between the optical and electrical aspects of the device owing to the large parasitic surface area related to the nanotextures, which may cause high surface recombination rates. Thus the low aspect-ratio nanostructures with effective optical-absorption enhancement, such as nanobowl [19], nanoinverted-pyramid [20] etc., are more effective for high-efficiency solar cells, especially for ultrathin c-Si where its physical thickness has become a critical constraint.

In this study the photon-capturing performance of c-Si TFSCs decorated with arrays of front nanobowls and rear truncated Ag nanopyramids are systematically evaluated and optimized via full-wave finite-element simulation. Our results show that light reflection of the device and parasitic absorption in the metallic reflector are clearly suppressed resulting in high optical absorption in almost the whole spectral band, which is comparable to the Yablonovitch limit. Besides, the ratio (m) of the periods between the rear and front nanstructures is regulated for further enhancement in optical absorption. Under a given set of electrical configuration and parameters, a thorough electrical evaluation indicates that light-conversion efficiency can be 15.51%, which is enhanced by 67.31% over its planar counterpart.

Figure 1(a) illustrates the schematic diagram of the proposed c-Si TFSCs, which are textured by the square arrays of front nanobowls (covered by a conformal SiO_2 antireflective/passivation layer) and a rear truncated

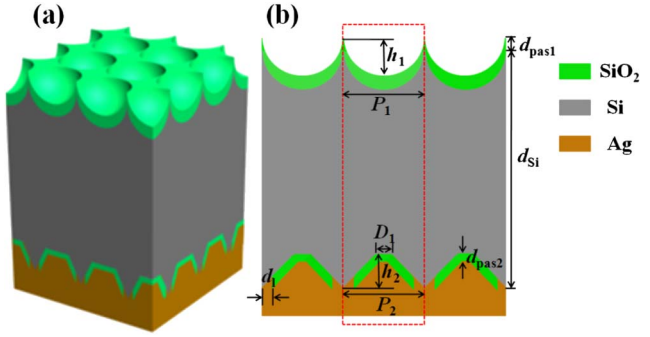

Fig. 1. (a) 3D visualization and (b) cross-sectional view of the proposed doubly-textured c-Si TFSCs.

nanopyramid Ag layer. The cross-sectional view of the device is shown in Fig. 1(b) where the characteristic sizes are defined. Considering that the involved parameters in the system are numerous, some of them are predefined empirically: $h_1 = h_2 = 300$ nm, $d_{pas1} = d_{pas2} = 100$ nm, $d_1 = 100$ nm, and $d_{Si} = 5$ μm. Moreover, we assume that $P_2 = mP_1$ where $m = 1, 2, 3\ldots$, and $D_1 = P_2/4$. Therefore only two parameters (i.e., P_2, m) are left to control and optimize the light-trapping performance of c-Si TFSCs. In this study the system will be compared to its planar counterpart, i.e., c-Si TFSCs with a 100 nm SiO_2 antireflective layer and an Ag rear reflector for discussion convenience.

The optical simulation is carried out by using the finite-element method (FEM) within the wavelength range (λ) between 300 and 1200 nm [21] where the wavelength-dependent refractive indices of the involved materials are from Palik's data [22]. To obtain an overall and quantitative evaluation of the photon-capturing capability of the c-Si TFSCs, the ultimate photocurrent density, J_{ph}, is calculated under an AM1.5 G solar spectrum [1,23].

Figure 2 shows the calculated J_{ph} as a function of P_2 under various values of m. It is shown that J_{ph} first increases and then decreases with increasing P_2 under all m configurations where the maximized J_{ph} values have been marked directly in the figure. The planar counterpart with an equivalent thickness is also plotted for comparison. Compared to the planar system where $J_{ph} = 24.75$ mA/cm^2, the doubly nanostructured systems exhibit substantially improved photocurrent density. They especially reveal that a larger m always yields a higher J_{ph}, e.g., when $m = 3$ and $P_2 = 1800$ nm, the maximum $J_{ph} = 35.29$ mA/cm^2 with an enhancement of 42.57% relative to the planar system.

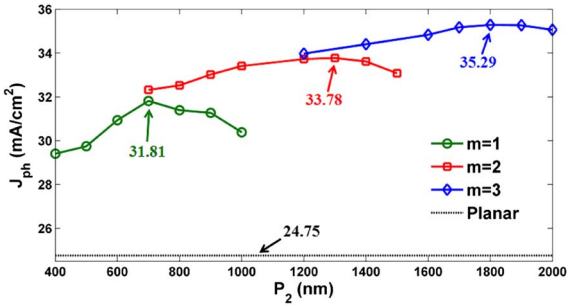

Fig. 2. J_{ph} versus P_2 under different m configurations where an equivalent planar system is plotted for reference.

It should be noted that $J_{ph} = 38.51$ mA/cm^2 under the Yablonovitch limit for the equivalent-thickness c-Si TFSCs shows that the proposed system can achieve a J_{ph} close to that of idealized Yablonovitch system [24].

To unveil the physics behind the dramatic enhancement of J_{ph} in the proposed TFSCs, the absorption (P_{Si}) and reflection responses are examined. Plotted in Fig. 3(a) are the P_{Si} spectra for various m setups under the respective optimal P_2, i.e., $P_2 = 700$, 1300, and 1800 nm for $m = 1$, 2, and 3, respectively. For comparison, the planar system is also included, which exhibits much lower absorption in almost the whole spectral range and strong cavity resonances excited from the well-shaped Fabry–Perot cavity. The full-band enhancement of the proposed system is the result of the combined effect from the front and rear nanostructures. It is also observed that the higher J_{ph} under a large m is not from the stronger cavity resonances in certain narrow spectral ranges but from a large broadband enhancement. The absorption spectrum of the Yablonovitch system is also displayed in order to better assess the photon-capturing performances of the proposed configuration. Although the absorption performance of the present design is still lower than that of the Yablonovitch limit, it is a more feasible system compared to previous idealized or extremely thin systems. As we have mentioned, the system has a number of controllable parameters and we choose to adjust only two of them for simplicity; therefore, even higher light-trapping performance can be achieved with a thorough optimization of the device parameters under a large m.

Figure 3(b) exhibits the absorption enhancement percentage (i.e., relative to the planar) of the system with $m = 3$. One can see that the enhancement rate when $\lambda < 580$ nm is relatively smooth, which is attributed to the high absorption coefficient and the antireflective effect of the front nanobowl layer. However, under longer wavelengths multiple sharp peaks are observed even in the range close to the band-edge of c-Si material. The sharp peaks stem from various kinds of optical resonances that arise from the hybrid cavity. To distinguish the role of front coating and the rear reflector in enhancing optical absorption the device reflection spectra for the planar, double nanostructure, and only front nanostructure designs are plotted in Fig. 3(c). It verifies that the front nanodesign leads to significantly suppressed

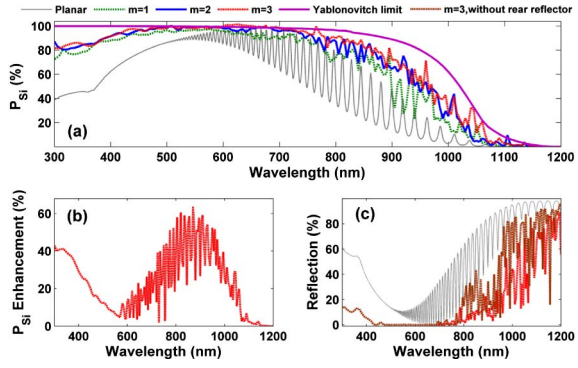

Fig. 3. (a) Absorption spectra of c-Si photoactive layer (P_{Si}), (b) P_{Si} enhancement, and (c) reflection spectra of the entire device.

reflection (from both the top and bottom interfaces under the metallic rear-reflector design) in the whole band when compared to the planar system. While further incorporating the rear plasmonic part, the device reflection is observed to be further reduced in the long wavelength band. This is because the optical absorption has been improved under the plasmonic effect.

Figures 4(a)–4(d) are the absorption profiles of the planar and optimized nanostructure designs (with $m = 1$, 2, and 3) at three representative wavelengths, i.e., $\lambda = 480$, 760, and 995 nm. At a short wavelength, e.g., $\lambda = 480$ nm, a high material-extinction coefficient of c-Si leads to strong light absorption at the region close to the cell surface; however, careful examination of the penetration depth shows that a front nanobowl design elongates the light path and improves the absorption. Under long wavelengths incident photons penetrate deeper into the c-Si photoactive layer, which leads to typical Fabry–Perot resonances in the planar system. However, the double-textured c-Si TFSCs behave in quite a unique way. First, it is obvious that the absorption efficiency is greatly improved and distributed in almost the whole photoactive region. Second, the absorption pattern is irregular compared to the planar setup. This is because the new system is composed by many rich interfaces and cavities instead of the standard multilayer cavity of the planar system. The complicated absorption patterns reflect the strongly intensified resonant modes excited from the new systems, facilitating light absorption in a broad spectral band. Third, the nanostructured design with a large m is accompanied by a high absorption density as shown in Figs. 4(b)–4(d), contributing to an improved absorption.

It is necessary to perform a thorough electrical evaluation on the designed c-Si TFSC. This is because in optical design J_{ph} is overestimated by assuming a perfect internal quantum efficiency (i.e., IQE = 100%); however, there are several kinds of carrier losses that lead to an imperfect IQE. The detailed optoelectronic simulation of typical solar cells can be found in [25–27]. However, it is quite challenging to realize a thorough three-dimensional (3D)

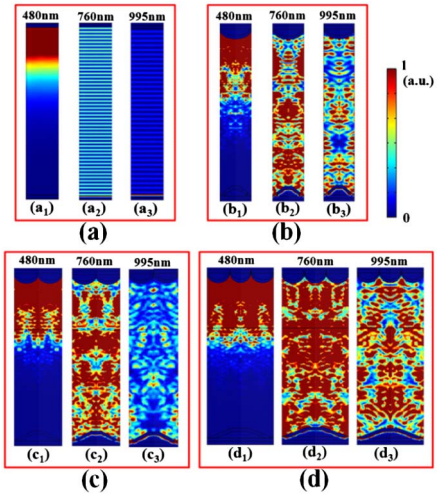

Fig. 4. Optical absorption profiles inside the c-Si TFSCs under (a) the planar and (b)–(d) the optimized nanostructure designs with $m = 1$, 2, and 3, respectively.

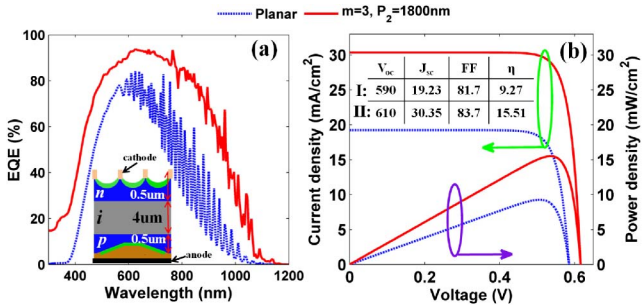

Fig. 5. (a) EQE spectra and (b) I-V characteristics of the c-Si TFSCs, where the planar and optimized nanostructured systems are considered. The optical configurations of the concerned systems have been given in the previous section and the electrical parameters are given in the main text.

electrical simulation to the proposed system due to the relative large thickness and complex device setup. Simplification can be realized by cutting the 3D system into many two-dimensional planes for electrical modeling only, and the overall electrical response takes their averages. Here, the carrier transport process is based on the photon-generated carrier from the optical simulation so such treatment does not modify the polarization dependence. Because the junction is along the vertical direction [see the inset of Fig. 5(a)] with very weak transverse dependence, we believe that such lateral discretization treatment can well reflect the actual response of the 3D system as long as the number of the planes is high enough (here 13 planes in one period).

The electrical parameters used in this study are as follows: the doping concentrations of p and n regions are 1.6×10^{20} (1×10^{18}) cm^{-3} and the thicknesses of p, i and n regions are 0.5, 4, and 0.5 μm [see the inset of Fig. 5(a)]; electron mobility in the $p/i/n$ region is 300/1100/100 cm^2/Vs, and hole mobility in the $p/i/n$ region is 160/420/160 cm^2/Vs the coefficients of Auger and bimolecular radiative recombinations are 9.9×10^{-32} (2.2×10^{-31}) cm^6/s and 9.5×10^{-15} cm^3/s, respectively. Other parameters are from [28]. Figure 5(a) shows the calculated external quantum efficiency (EQE) spectra of the c-Si TFSCs under planar and double-texture designs. It is seen that the EQE is significantly improved over that of the planar counterpart with the whole spectral range. Compared to the absorption spectra shown in Fig. 3(a), EQE is apparently lower than P_{Si} at the short wavelengths due to the strong surface and emitter recombination. At long-wavelengths, EQE shows a similar trend to P_{Si}. Figure 5(b) illustrates the current-voltage (J-V) characteristics of the above-mentioned two types of c-Si TFSCs under standard solar illumination (AM 1.5 G, 100 mW/cm^2). Compared to the planar system, the proposed device exhibits an increment ratio in short-circuit current density (J_{sc}) of 47.8%, a slightly increased open-circuit voltage (V_{oc}), and a significantly increased light-conversion efficiency (η) from 9.27% to 15.51%. However, the increases in V_{oc} and FF are quite small because they are determined primarily by the semiconductor and junction properties instead of the photonic design.

Under the given electrical configuration and parameters, the designed c-Si TFSC exhibits a good enough

electrical output. However, we would like to indicate that the electrical performance might be further improved by optimizing the corresponding system and semiconductor parameters.

In summary, we have proposed and evaluated (through electromagnetic and electrical simulation) a c-Si TFSC that is textured by the arrayed front nanobowls and truncated rear Ag nanopyramids. The new double-texture design leads to significantly enhanced optical absorption in a broad spectral band, owing to the joint effect of the improved front antireflection and the enhanced optical resonances between the front nanobowl and the rear nanopyramid layers. By properly designing the period ratio between the front- and rear-nanostructure layers, a maximal $J_{ph} \sim 35.29$ mA/cm^2 is obtained that is 42.57% higher than that of the planar reference. Under a defined set of electrical configuration for the new photovoltaic system, the realistic EQE and J-V responses were evaluated through addressing the detailed electron-hole interactions in the cell, predicting a light-conversion efficiency that has been improved from 9.27% (planar system) to 15.51%.

Finally, it should be indicated that other metals can be used for the plasmonic design proposed in this study, e.g., Au or Al, considering more properties including oxidation. We have conducted such simulations and found that the replacement of Ag by Au leads to similar performance; however, rear Al plasmonic design shows a relatively lower performance compared to the others. This provides us more options for highly efficient thin-film photovoltaic devices under various plasmonic designs.

This work was supported by National Natural Science Foundation of China (Nos. 61204066, 91233119, 61404144, and 61405132), Natural Science Foundation of Jiangsu Province of China (Nos. BK20141200 and BK20140349), and Priority Academic Program Development (PAPD) of Jiangsu Higher Education Institutions.

References

1. J. Gjessing, E. S. Marstein, and A. Sudbø, Opt. Express **18**, 5481 (2010).
2. J. Gjessing, E. S. Marstein, and A. Sudbø, J. Appl. Phys. **110**, 033104 (2011).
3. S. E. Han and G. Chen, Nano Lett. **10**, 4692 (2010).
4. J. S. Li, H. Y. Yu, Y. L. Li, F. Wang, M. F. Yang, and S. M. Wong, Appl. Phys. Lett. **98**, 021905 (2011).
5. S. Pillai, K. R. Catchpole, T. Trupke, and M. A. Green, J. Appl. Phys. **101**, 093105 (2007).
6. P. Matheu, S. H. Lim, D. Derkacs, C. McPheeters, and E. T. Yu, Appl. Phys. Lett. **93**, 113108 (2008).
7. Y. M. Song, J. S. Yu, and Y. T. Lee, Opt. Lett. **35**, 276 (2010).
8. X. Li, C. Zhang, Z. Yang, and A. Shang, Opt. Express **21**, A677 (2013).
9. R. Y. Zhang, B. Shao, J. R. Dong, J. C. Zhang, and H. Yang, J. Appl. Phys. **110**, 113105 (2011).
10. M. Wellenzohn and R. Hainberger, Opt. Express **20**, A20 (2012).
11. H. A. Atwater and A. Polman, Nat. Mater. **9**, 205 (2010).
12. W. L. Bai, Q. Q. Gan, F. Bartoli, J. Zhang, L. K. Cai, Y. D. Huang, and G. F. Song, Opt. Lett. **34**, 3725 (2009).
13. R. Dewan, I. Vasilev, V. Jovanov, and D. Knipp, J. Appl. Phys. **110**, 013101 (2011).
14. Z. Yang, A. Shang, Y. Zhan, C. Zhang, and X. Li, Opt. Lett. **38**, 5071 (2013).
15. R. Biswas and C. Xu, Opt. Express **19**, A664 (2011).
16. V. E. Ferry, A. Polman, and H. A. Atwater, ACS Nano **5**, 10055 (2011).
17. K. X. Wang, Z. F. Yu, V. Liu, Y. Cui, and S. H. Fan, Nano Lett. **12**, 1616 (2012).
18. Y. P. Shi, X. D. Wang, W. Liu, T. S. Yang, J. Ma, and F. H. Yang, Opt. Express **22**, 20473 (2014).
19. P. Q. Gao, H. Z. Wang, Z. X. Sun, W. Q. Han, J. S. Li, and J. C. Ye, Appl. Phys. Lett. **103**, 253105 (2013).
20. A. Mavrokefalos, S. E. Han, S. Yerci, M. S. Branham, and G. Chen, Nano Lett. **12**, 2792 (2012).
21. Comsol Multiphysics, http://www.comsol.com/.
22. E. D. Palik, *Handbook of Optical Constants of Solids* (Academic, 1985), p. 286.
23. ASTM, http://rredc.nrel.gov/solar/spectra/am1.5.
24. E. Yablonovitch, J. Opt. Soc. Am. **72**, 899 (1982).
25. X. Li, N. Hylton, V. Giannini, K.-H. Lee, N. J. Ekins-Daukes, and S. A. Maier, Opt. Express **19**, A888 (2011).
26. X. Li, N. Hylton, V. Giannini, K.-H. Lee, N. J. Ekins-Daukes, and S. A. Maier, Prog. Photovoltaics **21**, 109 (2013).
27. X. Li and Y. Zhan, Appl. Phys. Lett. **102**, 021101 (2013).
28. Y. Zhan, X. Li, and Y. Li, IEEE J. Sel. Top. Quantum Electron. **19**, 4000208 (2013).